Quick Prediction of Losses During Magnetization State Changes in Variable Flux Machines

Julius Kesten
Institute of Electrical Engineering
Karlsruhe Institute of Technology
Karlsruhe, Germany
julius.kesten@kit.edu

Martin Doppelbauer
Institute of Electrical Engineering
Karlsruhe Institute of Technology
Karlsruhe, Germany

***Abstract*—In order to effectively estimate the additional energy required to change the magnetization state in a variable flux machine, this process needs to be characterized as precise as possible and as quick as possible. Therefore, a loss estimation model for magnetization state changes based on a mix of FEA data and analytical calculations for the iron, copper and magnet losses in variable flux machines is presented and evaluated in this paper. Also, an approach to quickly estimate the current pulse required to set a desired magnetization state is derived. The loss model allows predictions that are much faster than FEA calculations with good accuracy.**

***Index Terms*—variable flux machine, memory machine, magnetization state change, loss estimation, permanent magnet synchronous machines**

I. Introduction

The permanent magnet flux in variable flux machines (VFM) as described in [1] can be controlled by applying appropriate stator current pulses. Therefore VFM can achieve high efficiencies, especially in the field weakening range.
If a VFM is to be used in traction applications, a large portion of its operating range is utilized more dynamically than in an industrial drive, for example. To achieve high overall efficiency in a given drive cycle for an electric vehicle both the optimal flux level for each operating point in the cycle as well as the required energy to apply that required flux level need to be calculated quickly and precisely. The focus of this work lies on the latter goal, i.e. the prediction of magnetization state (MS) change losses. The estimation of these losses is crucial for the control strategy in such machines, as the gain in efficiency during field weakening operation is directly influenced by the cost, i.e. the energy required to change the MS. While the design of VFM has been described and many propositions on design approaches have been made, namely in [2], [3], [4] and [5], only few authors consider the magnetization energy estimation. Furthermore, the machines presented in [2] - [4] focus on different than traction applications, as they usually have little to no reluctance torque and rely on magnet topologies employing single magnets. This allows accurate control of the MS, but does not yield the power densities required for traction machines.
In [6] an approach using FEA simulations is presented and verified using measurements. However, the estimation requires an FEA calculation for every change in MS and is therefore rather time consuming. Another of the few publications dealing with this issue is [7], where the MS of the machine is estimated using the flux change rate calculated from the applied voltage and the current response. This information is not used to calculate the required energy or the losses occurring during a MS change.
Therefore, a quick prediction model for both demagnetization and re-magnetization is presented in this work. The model considers the additional copper, iron and magnet losses occurring during the MS state change, revealing the total amount of losses as well as their origin within the machine. Additionally, a means of controlling the flux in VFM topologies with multiple low coercive field magnets is investigated using the relation between the permanent magnet flux Ψ_{PM} and the magnets' flux density.

This work was part of the research project "ReMos 2" ("Effiziente Reluktanzmaschine für effiziente Mobilität ohne seltene Erden 2"), financed through the Ministry of Science, Research, and Arts of the Federal State of Baden-Württemberg in the framework of "Innovationscampus Mobilität der Zukunft".

II. Modeling

A. Machine Under Investigation

The machine design presented in [5] is investigated in this work. They key features of this machine are summarized below in table I. An important distinction between this machine and other VFM is the magnet topology as depicted in Fig. 1. Instead of one low coercive field magnet as presented in [8] or hybrid constructions using single low coercive field magnets in arrays with high coercive field ones like in [4] and [2] there are three low coercive field magnets, one in each of the flux barriers.

TABLE I: Characteristics of machine under investigation

Characteristic	Value
No. of poles	6
No. of slots	36
Magnet material	AlNiCo9
Electric sheet material	NO-30
Maximum current (A)	300
DC link Voltage (V)	400

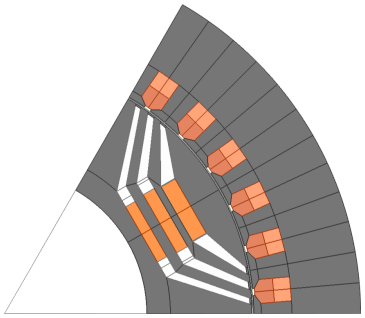

Fig. 1: Cross-section of the machine under investigation

This topology improves torque production compared to other VFM types, but controlling the magnets' flux is more difficult as they are not demagnetized evenly, as is depicted in Fig. 2. The upper part of the figure shows the flux density distribution in the rotor before an MS change current is applied. The lower cross section shows the rotor in the same operating point, but after the MS change has occured. As becomes clear from this, the individual magnets are hard to demagnetize and remagnetize evenly.

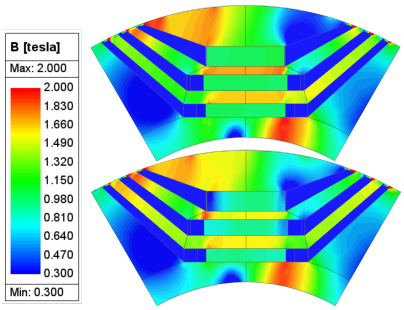

Fig. 2: Effect of MS changes on the individual magnets

The machine's performance characteristics are calculated based on FEA simulations, which are performed for a single speed of $10\,000\,1/\mathrm{min}$ and full magnetization $\Psi_{\mathrm{PM}} = 100\%$ with 11 steps in the current angle φ and 8 steps in the current I_{rms} axis, yielding 8×11 matrices for the key data such as flux linkages, losses, torque, external fields acting on each magnet, etc.

B. Magnetization State Change Current Estimation

The magnetization state change in the machine is achieved through current pulses of the d-axis current i_{d}. To find the appropriate magnitude of these current pulses, it is necessary to relate the required flux level to the d-axis current. The q-axis current i_{q} is assumed to be constant during the MS change process. Both the PM flux Ψ_{PM} and the external fields H acting on the magnets are known through the FEA simulations described above. Therefore, an airgap line of Ψ_{PM} can be given, as shown in Fig. 4. The maximum value of Ψ_{PM} is defined as Ψ_{100}. Using the value of the field strength H corresponding to Ψ_{100}, the relative flux density B_{100} is also defined, describing the no-load flux density, i.e. the magnets' working point when only subjected to the reluctance of the machine's magnetic circuit as a load.

The field strength required to achieve a certain Ψ_{PM} can be estimated by finding the intersection between the recoil line and the magnet specific material curve, e.g. the B-H-curve. The recoil line is given as

$$f_{\mathrm{RL}} = \mu_{\mathrm{lin}} \cdot x + B_{\mathrm{y}} \tag{1}$$

with the recoil permeability μ_{lin} and the y-intercept B_{y}, which is to be determined for each flux level, and the magnets' BH curve f_{BH}. The airgap line with respect to Ψ_{PM} is defined as

$$f_{\mathrm{AG},\Psi} = \frac{\Psi_{100}}{H_{100}} \cdot x. \tag{2}$$

When a new Ψ_{PM} is to be set, the corresponding value of the magnetizing field H_{x} is calculated using f_{AG}. The value of H_{x} is then used to find the relative flux density B using $f_{\mathrm{AG,B}}$, which is defined similarly to (2). Now, the y-intercept B_{y} of f_{RL} is known and the function is fully defined. By solving the linear equation

$$f_{\mathrm{RL}} = f_{\mathrm{BH}} \tag{3}$$

the sought after field strength is finally determined. The corresponding current value is then found from the H-I-φ lookup table. Since the outermost magnet is subjected to the largest magnitudes of external fields and also has the greatest area - and therefore contributes most to Ψ_{PM} - the fields acting on this magnet are considered for the current estimation [9]. This approach allows an estimation of the required MS change current using only two sets of FEA data: one for $\Psi_{\mathrm{PM}} = 100\%$ and one for $\Psi_{\mathrm{PM}} = 0\%$, because the airgap line can be assumed to be linear in a good approximation.

C. Loss Calculation

The iron losses are estimated using look-up tables which are generated using the same set of simulation data from which the H-I-φ matrix was generated, see chapter II. The loss data for the stator iron losses $P_{\mathrm{Fe},1}$ and the rotor iron losses $P_{\mathrm{Fe},2}$ are each interpolated within the given I-φ-plane using a cubic interpolation in MATLAB. The speed dependent loss adjustment is done using a modification of Bertotti's model, where there are only two of the original three iron loss components, namely the eddy current P_{cls} and the excess loss P_{exc} ones

$$\begin{aligned} P_{\mathrm{Fe}} = P_{\mathrm{cls,nom}} \left(\frac{f}{f_{\mathrm{nom}}}\right)^2 \left(\frac{B}{B_{\mathrm{nom}}}\right)^2 + \\ P_{\mathrm{exc,nom}} \left(\frac{f}{f_{\mathrm{nom}}}\right)^{3/2} \left(\frac{B}{B_{\mathrm{nom}}}\right)^{3/2}, \end{aligned} \tag{4}$$

where the $P_{\mathrm{cls,nom}}$ and $P_{\mathrm{exc,nom}}$ denominate the eddy current and excess losses, respectively, and the index nom represents the nominal value, at which the corresponding quantity (i.e. the losses P_{Fe}, frequency f or flux density B) was originally recorded [10].

The hysteresis losses are considered by fitting the eddy current and excess loss coefficients accordingly. This is

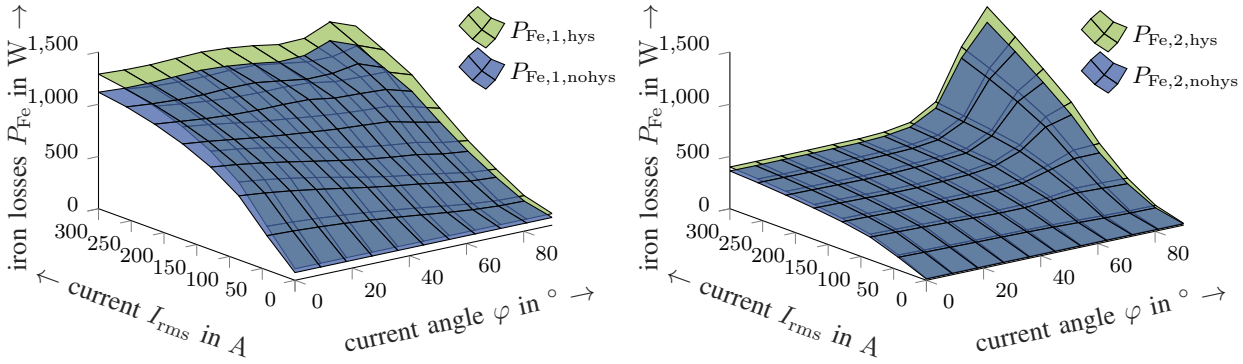

(a) stator losses

(b) rotor losses

Fig. 3: Comparison of iron losses with and without hysteresis coefficient

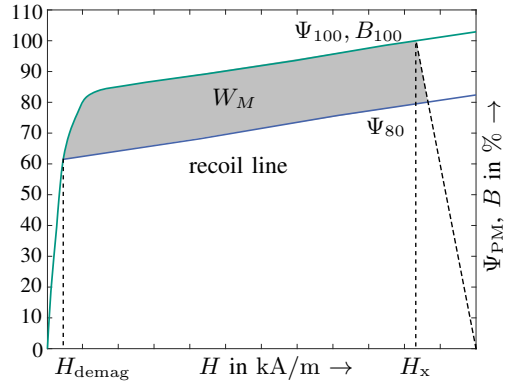

Fig. 4: Lookup of Ψ-H-relation

necessary to keep simulation times small, since the employed software, Ansys Electronics, simulates the hysteresis losses as if the electric sheets were magnetized initially and therefore would require an entire electric period until the calculated losses reach their actual value. By using the fitting method mentioned above, this is avoided and the FEA simulation needs consider only $1/6$ of an electrical period. The result of the fit is presented in Fig. 3 for both the losses in the stator and the rotor. While the fitted model - represented by the green surface - estimates the losses slightly higher than the classic approach, presented in green, there is a good agreement between both datasets, allowing this approach to be employed in the loss estimation model.

The losses occurring during each timestep of the demagnetization process are derived by interpolating between the sample points in the I-φ plane provided by the data represented in Fig. 3.

The magnets' eddy current losses are estimated using the same principle, while the hysteresis losses of the magnets are not provided via the FEA simulations. A different approach is therefore required to achieve a description of this loss component.

The energy W_{M} dissipated in a magnet due to its hysteresis is given as the volume integral of the circulation of the magnetic field strength H via the flux density B

$$W_{\mathrm{M}} = \int_{\mathrm{V}} \underbrace{\left[\oint H \, \mathrm{d}B \right]}_{w_{\mathrm{m,hys}}} \mathrm{d}v \tag{5}$$

with the magnet's Volume V. The energy is represented by the grey area in Fig. 4. With the knowledge of the initial magnetization state, the applied external field H_{ext} and the consideration of the magnets' constant volume, the MS change energy for the magnets' hysteresis loss can be calculated.

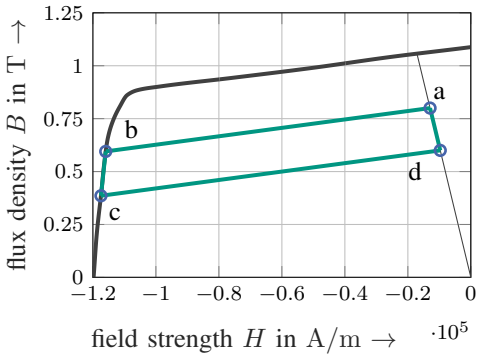

Fig. 5: Magnet hysteresis loss calculation

In Fig. 5 the integration takes place along the curve given by points a, b, c and d. In order to correctly calculate the hysteresis losses occurring during the MS change, each section of the curve is calculated separately. The total energy density $w_{\mathrm{m,hys}}$ as given by the inner integral in (5) is achieved through

sign correct addition of the partial integrations.

$$w_{\mathrm{m,hys}} = \int_{B(a)}^{B(b)} f_{\mathrm{RL}}|_{ab}\,\mathrm{d}B + \int_{B(b)}^{B(c)} f_{\mathrm{BH}}\,\mathrm{d}B - \int_{B(c)}^{B(d)} f_{\mathrm{RL}}|_{cd}\,\mathrm{d}B + \int_{B(d)}^{B(a)} f_{\mathrm{AG}}\,\mathrm{d}B \tag{6}$$

In (6), the flux densities $B(x)$ in the integrals' limits describe the flux density on either the magnets' BH curve f_{BH}, the recoil line f_{RL} or the airgap line f_{AG}, respectively. Fig. 6 shows the inverted BH curve where the field strength H is a function of the flux density B.

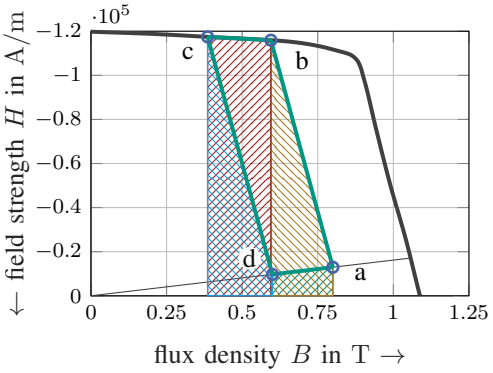

Fig. 6: Magnet hysteresis loss calculation inverse

The areas described by each integral in (6) are hatched and colored differently to illustrate the choice of sign in the summation. Should the MS change starting point (a) lie on the major hysteresis loop, the integral $\int_{B(a)}^{B(b)}$ is replaced by one along that outer loop accordingly. The hatched areas below the magnets' airgap line f_{AG} are displayed for the sake of clarity only as the actual hystersis losses occurring are represented by the area within $\overline{abcd}$. The magnets' airgap line is required for this calculation and can is taken from the FEA data mentioned above.

The copper losses are estimated using the current and the stator resistance R_{S}. Since the q-axis current is assumed to be constant, the additional copper losses P_{Cu} occurring during the process are attributed to i_{d} only and are therefore given as

$$P_{\mathrm{Cu}} = 3 \cdot R_{\mathrm{S}} \cdot i_{\mathrm{d}}^2. \tag{7}$$

III. Results

The currents required for different MS changes are estimated using the approach described in section II-B. Table II shows the estimated i_{d} values and the achieved MS $\Psi_{\mathrm{PM,sim}}$ for different reference magnetization levels $\Psi_{\mathrm{PM,ref}}$. The q-current is adjusted in accordance with the values given in the table. The nominal value of the PM flux is $\Psi_{\mathrm{PM}} = 0.0476\,\mathrm{Vs}$. The time dependency of the d-current is simplified to a trapezoid as represented in Fig. 7.

TABLE II: MS change estimation results

$\Psi_{\mathrm{PM,ref}}$ (%)	i_{q} (A)	$i_{\mathrm{d,est}}$ (A)	$\Psi_{\mathrm{PM,sim}}$ (%)
80	100	-97.04	83.8
60	50	-163.6	54.6

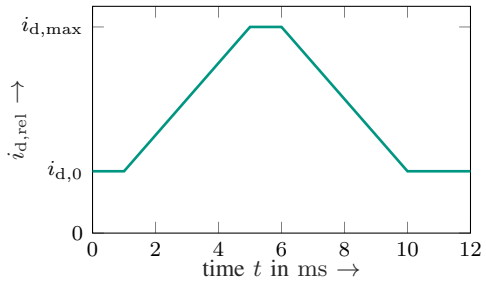

Fig. 7: d-current slope with normalized current

As becomes clear from table II, the presented estimation method for the flux gives acceptable results, but is prone to a certain margin of error. This is due to the high number of parameters influencing the final MS. The results presented for the loss estimation are therefore presented using the general time dependency of the d-current, as shown in Fig. 7, with given values for the d- and q-currents.

Three exemplaric working points are therefore selected. The working points' data is summarized in table III. Starting point for each MS change presented here is a fully magnetized machine, i.e. $\Psi_{\mathrm{PM}} = 100\%$.

All model results shown below are based on a single set of FEA data given in the form of an 8×11-matrix as described in chapter II-A. The data labeled simulation in this chapter is generated by performing FEA analyses with the current slope presented in Fig. 7 and the data from table III. The simulations are carried out using a resolution of 108 samples per electrical period.

TABLE III: loss estimation working points

id #	n (1/min)	i_{q} (A)	$i_{\mathrm{d,0}}$ (A)	$i_{\mathrm{d,max}}$ (A)
WP_1	7500	100	-50	-135.4
WP_2	10000	50	-75	-157.1
WP_3	12500	50	-25	-161.5

A. Time-Dependent Loss Power

The copper losses are calculated according to (7), taking into consideration only the additional copper losses resulting from the MS change d-axis current. The result of this calculation is shown in Fig. 8. The results presented in this figure as well as the time dependent curves presented in Fig. 9 are averaged over one electrical period. This allows for better comparability between the model and the simulation results, since the non-averaged data is very scattered due to the high harmonic content in the simulated loss.

The maximum loss in Fig. 8 is largest for WP_3, since the

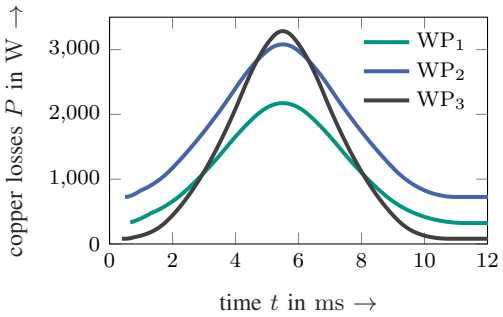

Fig. 8: Copper losses for the different working points

d-current $i_{\mathrm{d,max}}$ reaches its highest value in this working point. Since this loss component is calculated analytically from an estimate of the winding resistance R_{S}, the results can not be compared to any FEA data.

Fig. 9 shows the estimated losses as found by the model in comparison with the simulated losses for the current slope presented in Fig. 7. The in curves printed in full lines in this figure represent the model values, while the dash-dotted lines represent the simulated values. As is visible in the figure, the model overestimates the peak loss power occurring during the MS change operations, but tends to yield lower results at the flanks of the curve for all WP. WP$_1$ shows the weakest model performance, the peak of the model curve appears to be shifted slightly to the right compared to the simulated curve in all subfigures. The overall trend of the maximum loss power occurring for each WP is as expected from (4), showing increasing loss with rising frequencies.

B. Loss Energy

Because loss as an instantaneous value has limited informative value for the desired cycle energy estimation this research is aimed at, the loss energy derived from the time integral of the loss power shown above, is presented for the copper and iron losses, as well as the magnets' hysteresis loss. For the latter there is no time-dependent representation, as the integral in (5) is solved for the energy directly. All integrations of time-dependent quantities took place only in between $t_0 = 1\,\mathrm{ms}$ and $t_1 = 12\,\mathrm{ms}$. This represents the time interval during which the additional losses due to the MS change occur. Also, for these calculations, none of the data was averaged.

Fig. 10 shows the loss energy for both copper an PM losses in all WP. In comparison to Fig. 8, the maximum loss energy does not occur for WP$_3$, like the maximum loss power, but for WP$_2$. This is due to the larger area beneath the loss power curve of WP$_2$ as a consequence of the larger starting current $I_{\mathrm{rms},0}$.

The values of the magnets' hystersis loss increase from WP$_1$ to WP$_3$, as do the values of the MS change current, which relates directly to the demagnetizing field, as described in chapter II-B.

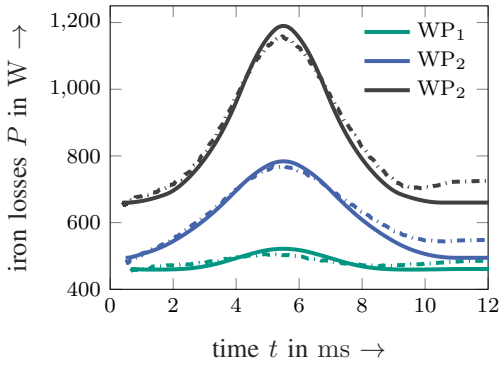

(a) stator losses

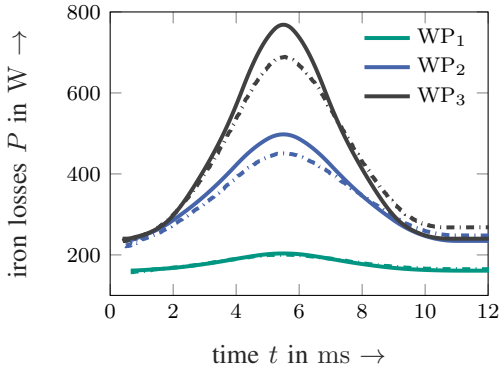

(b) rotor losses

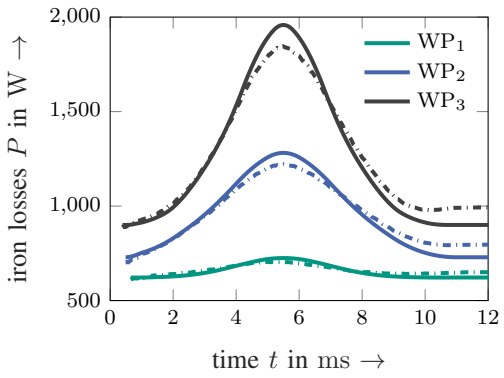

(c) total losses

Fig. 9: Iron loss power in rotor and stator for the investigated working points

For the iron loss energy, the representation is split into stator and rotor, as well as eddy and excess loss, to also give an illustration of how the loss power presented in Fig. 9 is distributed between the two remaining loss components, as can be seen in Fig. 11.

The stator loss energy is estimated too low by the model for all WP, while the rotor loss energy is estimated too high. For the stator losses, the major component is the excess one, which is attributed to the presented simplification in Bertotti's loss model. Since there is no hysteresis loss coefficient, a large part of the hysteresis loss is included in the excess loss. This

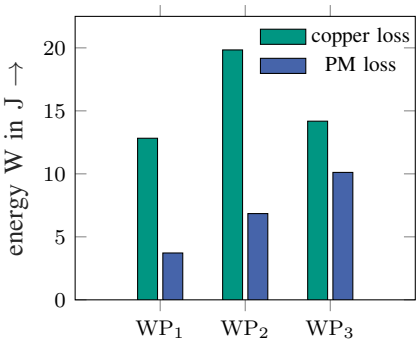

Fig. 10: Copper and magnet hysteresis loss for the investigated working points

TABLE IV: Model prediction error

	error in %		
loss component	WP_1	WP_2	WP_3
stator eddy losses	-0.31	-1.60	-1.84
stator excess losses	-1.01	-2.50	-2.64
rotor eddy losses	0.01	4.70	2.75
rotor excess losses	-0.11	3.63	2.31
total stator losses	-0.74	-2.12	-2.30
total rotor losses	-0.05	4.15	2.54
total iron losses	-0.55	0.04	-0.71

is also evident when investigating the rotor losses: Here, the excess loss contributes about half or less to the overall loss energy, since there is typically less hystersis loss in the rotor compared to the stator.

To quantify the accuracy of the modeling approach, table IV gives an overview of the relative model error for the data presented in Fig. 11. As can be seen from table IV the prediction error is less than 5% for all operating points investigated. Further, the error for the total iron loss energy occurring during MS change operations is smaller than 1%. Even for WP_1 with the least accurate prediction of the time-dependent loss power the error in the energy estimation is small.

IV. Conclusion and Future Work

A quick prediction method for the required MS change currents and the MS change losses based on two FEA datasets describing a machine's characteristics was presented. Since only few FEA calculations are necessary for modeling, the prediction of the current magnitude and the losses is time efficient.

The estimated currents i_d result in values of Ψ_PM that differ up to 10% from the required value $\Psi_{\mathrm{Pm,ref}}$. Further investigations need to be carried out, to control the expected flux more precisely. This could be achieved by considering the uneven change in MS between the magnets in total and for each magnet individually, for example. While the main goal of the approach presented here was to create a model that requires as few FEA calculations as possible, it might be necessary to increase the number of calculations on which the MS change current estimation is based to achieve more precise results.

The prediction of the copper, iron and magnet losses during MS changes was implemented and results for three working points were presented and discussed. While the copper and magnet losses are calculated analytically and can therefore not be compared to FEA data, the iron losses show exact prediction results. This allows the implementation of this model into an overall optimization strategy for the use of VFM in traction applications. To utilize this model to its full extent, a VFM prototype will be built and the iron loss characteristics of that machine will be recorded. Using the measured data, the

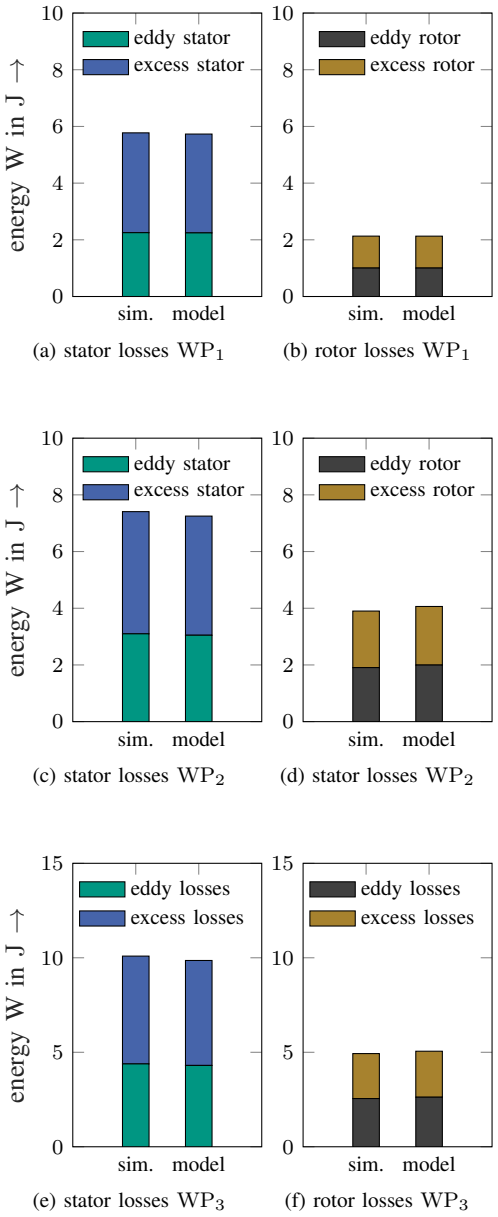

(a) stator losses WP_1 (b) rotor losses WP_1

(c) stator losses WP_2 (d) stator losses WP_2

(e) stator losses WP_3 (f) rotor losses WP_3

Fig. 11: Iron loss energy in rotor and stator for the investigated working points

prediction quality of the model can be refined further.
However, the losses energies found by the model appear to be small compared to the energy turnover of a middle class car in the WLTP cycle, which is about $12.8\,\mathrm{kJ}$ for a 2017 Volkswagen Golf, meaning that MS change losses will probably only have little part in overall losses.
In further steps, a model to predict the efficiency optimal flux level for a given operating point is to be developed so that drive cycle optimizations can be carried out without recalculating a machine's full characteristics. Based on those results, different control strategies will be investigated and compared, e.g. intelligent MS controllers that calculate the required flux level from a route given to them by a navigation software, for example, or simpler controllers, such as hysteresis based MS controllers that generate the MS change command simply based on the machine's current operating point.

REFERENCES

[1] V. Ostovic, "Memory motors," *IEEE Industry Applications Magazine*, vol. 9, no. 1, pp. 52–61, 2003.

[2] K. Sakai, K. Yuki, Y. Hashiba, N. Takahashi, and K. Yasui, "Principle of the variable-magnetic-force memory motor," in *2009 International Conference on Electrical Machines and Systems*. IEEE, 112009, pp. 1–6.

[3] M. Ibrahim, L. Masisi, and P. Pillay, "Design of Variable-Flux Permanent-Magnet Machines Using Alnico Magnets," *IEEE Transactions on Industry Applications*, vol. 51, no. 6, pp. 4482–4491, 2015.

[4] Y. Zhou, Y. Chen, and J.-X. Shen, "Analysis and Improvement of a Hybrid Permanent-Magnet Memory Motor," *IEEE Transactions on Energy Conversion*, vol. 31, no. 3, pp. 915–923, 2016.

[5] J. Kesten, F. Frölich, F. Wittemann, J. Knirsch, F. Bechler, L. Kärger, P. Eberhard, F. Henning, and M. Doppelbauer, "Design Approach for a Novel Multi Material Variable Flux Synchronous Reluctance Machine without Rare Earth Magnets," in *2022 International Conference on Electrical Machines (ICEM)*. IEEE, 952022, pp. 2304–2310.

[6] A. Takbash and P. Pillay, "Magnetization and Demagnetization Energy Estimation and Torque Characterization of a Variable-Flux Machine," *IEEE Transactions on Energy Conversion*, vol. 33, no. 4, pp. 1837–1845, 2018.

[7] Y. Hu, J. Chen, R. Qu, B. Chen, Y. Xiao, and X. Li, "Closed-Loop Magnetization State Control for a Variable-Flux Memory Machine," *IEEE Access*, vol. 8, pp. 146 983–146 993, 2020.

[8] M. Ibrahim and P. Pillay, "Design of Hybrid Variable Flux Motors for Enhanced Wide-Speed Performance," in *2019 IEEE Energy Conversion Congress and Exposition (ECCE)*. IEEE, 29.09.2019 - 03.10.2019, pp. 6046–6053.

[9] T. A. Huynh, M.-F. Hsieh, K.-J. Shih, and H.-F. Kuo, "An Investigation Into the Effect of PM Arrangements on PMa-SynRM Performance," *IEEE Transactions on Industry Applications*, vol. 54, no. 6, pp. 5856–5868, 2018.

[10] G. Bertotti, "General properties of power losses in soft ferromagnetic materials," *IEEE Transactions on Magnetics*, vol. 24, no. 1, pp. 621–630, 1988.

Julius Kesten received his B.Sc. and M.Sc in Mechatronics and Information Technology in 2016 and 2020 from the Karlsruhe Institute of Technology (KIT), Germany. Since 2020 he works as research assistant at the Institute of Electrical Engineering at the KIT. His research interests include the design of synchronous reluctance and variable flux machines as well as the numerical optimization of electric machines.

Martin Doppelbauer is full professor since 2011 at the Institute of Electrical Engineering (ETI) at the Karlsruhe Institute of Technology (KIT) in Karlsruhe, Germany. He holds a chair for Hybrid Electric Vehicles. Prior to that, he worked in industry for 15 years, most recently as head of electrical machine development at SEW Eurodrive GmbH in Bruchsal. Martin Doppelbauer is also active in national and international standardization. He is the chairman of IEC Technical Committee 2 Rotating Electrical Machines.